



Preparation and Magnetic Properties of NiFe₂O₄ Plate Nanoparticles

FERAY KOCAN ^{1,2}

1.—Faculty of Arts and Sciences, Chemistry Department, Manisa Celal Bayar University, 45140 Yunusemre, Manisa, Turkey. 2.—e-mail: feraykocan45@gmail.com

The aim of this study was to investigate nickel ferrite (NiFe₂O₄) plate nanoparticles synthesized by the co-precipitation method. The effects of parameters such as solution pH and Fe³⁺/Ni²⁺ mole ratio of nickel ferrite nanoparticles were analyzed. The nanoparticles synthesized by the co-precipitation method were calcined at 650°C. The samples were characterized by x-ray diffraction (XRD), scanning electron microscopy (SEM), energy dispersive x-ray analysis (EDAX), and Fourier-transform infrared spectroscopy (FTIR). The remanent magnetization, saturated magnetism, and coercivity properties of the samples were measured with a vibrating sample magnetometer (VSM). In a synthesis process with Fe³⁺/Ni²⁺ = 1 mole ratio, a Ni_{1.43}Fe_{1.7}O₄ compound was formed where NiFe₂O₄ was expected to form. NiFe₂O₄ plate nanoparticles with 108-nm particle size were successfully synthesized using the Fe³⁺/Ni²⁺ = 2 mole ratio.

INTRODUCTION

Nanocrystal ferrites, which have the general formula MFe₂O₄ (M: Ni, Co, Mn, Cu, Mg, Cd, Zn, etc.), constitute one of the most striking material classes in technological applications.^{1,2} Nickel ferrites (NiFe₂O₄) crystallize in the cubic crystal system and are reverse spinel materials with the general formula A²⁺B₂³⁺O₄²⁻. Cation distributions are found in octahedral and tetrahedral regions.³ Due to their high electrical resistance, high permeability, and low eddy losses in the electromagnetic field, nickel ferrites are used in many technological applications, such as high-density magnetic storage devices, microwave devices, telecommunication equipment, magnetic fluids, pharmaceutical production, gas sensors,^{4–7} moisture sensitive sensors, and electrical, electronic, and catalytic applications.⁸ In addition, ferrite nanoparticles decrease water pollution due to their photocatalytic effect gained by absorbing UV rays.⁹

Nickel ferrites have various magnetic properties, such as paramagnetic, superparamagnetic, and ferrimagnetic, depending on particle size and

shape.^{10,11} As the cation type changes, the particle size decreases to nanolevels, and ferrites with unexpected physical and chemical properties can be produced.^{12,13} The reduction in particle size leads to changes, such as the Neel temperature, higher coercivity, smaller saturation magnetization, and reduced or enhanced magnetic moments.^{14–17} Nickel ferrites are an important soft ferrite material due to their ferrimagnetic properties, low coercivity, low saturation magnetization, and high electrochemical stability.^{18–20}

The methods and conditions of the synthesis of ferrite materials strongly affect the properties of the sample, such as its size, shape, and morphology, and change the physical and chemical properties of the sample obtained.^{21,22} Many methods are used in the synthesis of nickel ferrites. These include coprecipitation,^{23,24} hydrothermal methods,^{25,26} sol-gel,^{27,28} solid-state reaction,^{12,29} microemulsion,³⁰ combustion,³¹ solvothermal,²² sonochemical,³² ultrasonic,³³ thermal decomposition (polyol),³⁴ and mechanical milling.³⁵ The co-precipitation method includes nucleation, growth, and coarsening and/or agglomeration processes. In this process, the nucleation of a large number of particles occurs after the solution is over-saturated. Another process, called Ostwald coarsening or agglomeration, dramatically affects the size, morphology, and properties of the samples.

This method can generate high-quality, high-purity, single- or multi-component metal oxides. If parameters such as the solution pH, reaction temperature, stirring speed, metal salt concentration, and surfactant concentration are carefully controlled, metal oxide particles of the desired shape and size can be produced without the need for any extra treatment, such as microwave heating or mechanical methods.³⁶ There are common problems, such as high temperature and low efficiency, in complex production processes, and the method used in production is one of the factors that most affects the composition and microstructure of the samples. The chemical coprecipitation method is simple and provides good particle size control.³⁷

The aim of this study was to synthesize pure nanosized nickel ferrite particles. The critical effects of parameters such as solution pH and mole ratio of Fe³⁺/Ni²⁺ on the sample were investigated in detail to control the shape and size of the nickel ferrites nanoparticles. The remanent magnetization, saturated magnetism, and coercivity properties of the samples were measured with a vibrating sample magnetometer (VSM).

EXPERIMENTAL

Materials

Analytically pure anhydrous iron (III) chloride (FeCl₃, Merck), nickel chloride hexahydrate (97%, NiCl₂·6H₂O; Merck), monoethanolamine (98%, HOCH₂CH₂NH₂; GPR), sodium chloride (NaCl; Merck), and sodium hydroxide (NaOH; Merck) were used to produce nickel ferrite nanoparticles. Deionized water was used in all the experiments. A thermometer (Isolab) with an accuracy of 1°C was used for measuring the temperature (−10 to 150°C). The temperature value was kept constant at 90°C in all the experiments.

Experimental Procedure

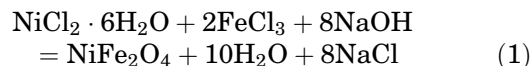
Experiments were conducted in a three-necked glass reactor placed in a water bath at 90°C. The solution was mixed with a mechanical stirrer at atmospheric pressure, and a condenser was used to prevent evaporation. The other neck of the reactor was closed with a stopper. The temperature of the solution in the reactor was continuously measured with a portable digital thermometer.

Synthesis of Nickel Ferrite Nanoparticles

A stoichiometric amount of ferric (III) chloride (FeCl₃) solid was added to distilled water at 90°C in a typical process. This solution was stirred at 500 rpm for 2 h to obtain ferric chloride solution. A stoichiometric amount of nickel (II) chloride hexahydrate (NiCl₂·6H₂O) was added to the iron chloride solution. This solution was stirred for 1 h at 500 rpm. After stirring for 1 h, a 5-M solution of sodium hydroxide (NaOH) was prepared and slowly

dropped into the mixture to adjust to the desired pH value. A dark brown precipitate appeared in the aqueous solution of Fe³⁺ and Ni²⁺ ions at a value of pH > 7. A 5-M solution and 20 mL of ethanolamine solution was dropped into the mixture.

The reaction is described by Eq. 1:



Filtration was performed, and the sample as precipitation was washed several times with distilled water and finally dried in an oven at a temperature of 50°C for 12 h. The dried samples were calcined at 650°C for 4 h.

CHARACTERIZATION

The crystalline structure of the NiFe₂O₄ nanoparticles was performed by x-ray diffraction (XRD) analysis on a Rigaku Ultima IV at a scanning rate of 1°/min with Cu-K α radiation in the range of 2 θ – θ from 10 to 90°. Scanning electron microscopy (SEM) and energy dispersive x-ray analysis (EDAX) were performed with an FEI Quanta-400F instrument. Magnetic measurements were carried out at room temperature using a Cryogenic PP MS VSM instrument. The function groups of the sample were investigated by Fourier-transform infrared spectroscopy (FTIR) spectra with a Perkin Elmer brand spectrum BX model in the range of 4000–400 cm^{−1} wavelength. The KBr solid pelletization method was used for the spectra.

RESULTS AND DISCUSSION

Effect of pH

The effect of the solution pH on the properties of morphology and shape of the nickel ferrite nanoparticles was investigated at pH values of 7, 8, 9, and 10. In the experiments, constant conditions of the solution were used, with a Fe³⁺/Ni²⁺ mole ratio of 2, a temperature of 90°C, and a 5-M ethanol amine concentration of 20 mL. The XRD patterns of the samples obtained from various pH values at 90°C are shown in Fig. 1. There are two phases, NiFe₂O₄

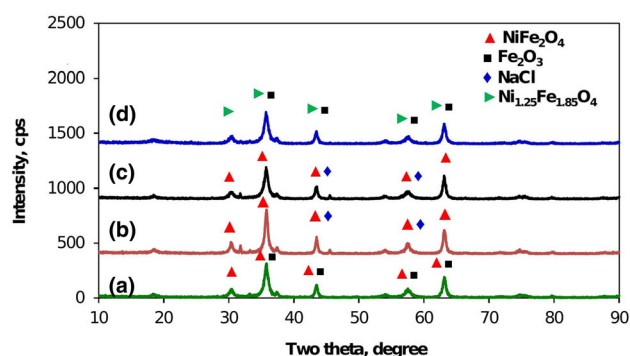


Fig. 1. XRD patterns at pH values: (a) pH = 7, (b) pH = 8, (c) pH = 9, and (d) pH = 10.

and Fe_2O_3 , in Fig. 1a and d, respectively. Additionally, the mixture of $\text{Ni}_{1.25}\text{Fe}_{1.85}\text{O}_4$ and NaCl is shown in Fig. 1b. It can be seen in Fig. 1a–d, respectively, that the four samples were obtained at different pH values and exhibited characteristic XRD peaks.

Figure 1a indicates the crystallinity and structure of the NiFe_2O_4 and Fe_2O_3 phases. The XRD pattern at pH = 7 has the impurity Fe_2O_3 as a by-product. In Fig. 1a, it can be seen that the ICDD card number of the NiFe_2O_4 peak is 540694, while the ICDD card number of the Fe_2O_3 peak is 330664. The first pH of the mixture is -0.20 . The pH slowly rises after NaOH is added drop by drop, and the color of the mixture changes from orange to brown as the pH of the solution is increased. As the pH reaches 7, the sample contains two phases.

In Fig. 1b, the sample was obtained at pH = 8, and two phases were observed, NiFe_2O_4 and NaCl. All the peaks of NiFe_2O_4 characterized are present: 30.30° (220), 35.76° (311), 37.33° (222), 43.45° (400), 53.80° (422), 57.52° (511), 62.92° (440), and 74.64° (533). The strong sharp peaks seen in Fig. 1b revealed that NiFe_2O_4 has a high crystallinity. The Fe_2O_3 phase which existed at pH = 8 has disappeared, and has been transformed to NiFe_2O_4 by increasing the alkalinity of the solution. It can be thought that NaCl is formed as an impurity in the sample, and that this is due to insufficient washing of the precipitate. In Fig. 1b of the pH = 8 samples, it can be seen that it was in good agreement with the NiFe_2O_4 ICDD 540964 card number and NaCl ICDD 750306 card number. The sample obtained at pH = 8 consisted of pure NiFe_2O_4 . Salavati-Nasari et al.,²⁴ in a study which synthesized nickel ferrite nanoparticles, ensured the removal of NaCl from the environment by washing the precipitate with distilled water and ethanol until the free sodium and chloride ions formed in the reaction medium were removed.

Figure 1c shows the XRD plot of the sample synthesized at pH = 9. Pure NiFe_2O_4 peaks can be observed, and no impurity peaks are detected. In the XRD analysis results of the sample, 18.37° (111), 30.30° (220), 35.76° (311), 37.33° (222), 43.45° (400), 57.52° (511), and 63.07° (440) planes can be observed. These planes are confirmed by the NiFe_2O_4 ICDD card number 540964 obtained from the XRD analysis belonging to the NiFe_2O_4 crystal. Sharp narrow peaks indicate that the sample crystallizes well. Impurity peaks were not observed in the XRD analysis. This can be attributed to the pure NiFe_2O_4 crystals that were synthesized. At pH = 8, NaCl is present as an impurity. During this experiment, pure NiFe_2O_4 crystals were obtained by washing the precipitate sufficiently. Therefore, pH = 8 and pH = 9 can be considered as optimal experimental conditions.

The pH value is a crucial factor affecting the morphologies, the crystal growth directions, and even the compositions of the samples. Shan et al.³⁸

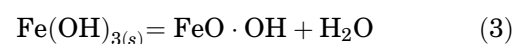
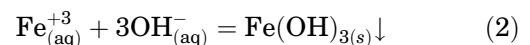
investigated the effects of pH = 5, 7, 12, and 13 on the phase transformations and morphologies of NiFe_2O_4 particles. It was stated that Fe^{3+} ions in the FeCl_3 compound in a pH = 5 acidic environment preferred a more stable state by forming $\alpha\text{-Fe}_2\text{O}_3$, and had rhombohedral morphology. However, it has been reported that Ni^{2+} ions in solution with the addition of NaOH prefer to form nickel ferrite, and show preferential growth during crystallization depending on the concentration of Ni^{2+} ions. It was observed that spherical NiFe_2O_4 nanoparticles were formed at pH = 7, nanorod particles at pH = 12 and nano=octahedron particles at pH = 13. Kumar and Bhowmik² stated that $\text{Ni}_{1.5}\text{Fe}_{1.5}\text{O}_4$ and a small amount of $\alpha\text{-Fe}_2\text{O}_3$ were formed at pH = 12 with the precipitation method, and that the most stable inverse spinel ferrites were stable between pH = 8 and 10, but surface defects occurred at extremely low and extremely high pH values. It has been reported that the distribution of Ni^{2+} and Fe^{3+} ions plays a crucial role in the formation of pH-dependent samples.

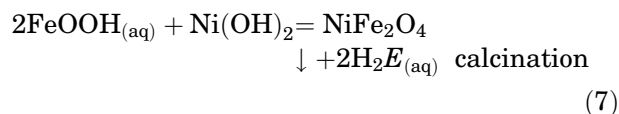
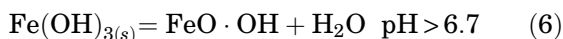
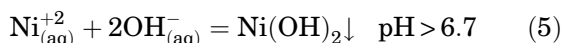
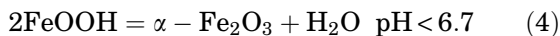
In Fig. 1d, $\text{Ni}_{1.25}\text{Fe}_{1.85}\text{O}_4$ ICDD (880380) and a small amount of $\alpha\text{-Fe}_2\text{O}_3$ ICDD (850599) were obtained at pH = 10, which is in agreement with the literature values.

In the literature, the solution pH affects the grain growth kinetics of the grains synthesized from the metal solution. However, there is no clear mechanism explaining the effect of pH change on the solution. Nonetheless, particle growth kinetics are controlled by the solution pH. The nucleation of particles is influenced by the existence of different types of cations, the Neel temperature, anions, their concentration, the composition and nature of the precipitated particles, and the interactions between the ions present in the solution. In an acidic environment, the concentration of H^+ ions is high, while, in an alkaline medium, the concentration of Na^+ ions is high. Since the mass and electric charge of H^+ ions are lower than those of Na^+ ions, the mobility of the H^+ ions is greater than that of the Na^+ ions. These differences affect the repulsive forces that control the nucleation and agglomeration of the particles.²

In conclusion, the pH strongly affects the structure of the sample obtained, with 108-nm nanoparticles obtained at pH = 8 in the presence of ethanolamine. In this study, it was decided that pH = 8 was the most suitable value.

Here, NaOH was used as a precipitation reagent to obtain nickel ferrite.³⁹ Fe^{3+} in FeCl_3 and Ni^{2+} in $\text{NiCl}_2 \cdot 2\text{H}_2\text{O}$ transform to $\text{Fe}(\text{OH})_3$ and $\text{Ni}(\text{OH})_2$, respectively, by adding NaOH. The solubility products of $\text{Fe}(\text{OH})_3$ and $\text{Ni}(\text{OH})_2$ are 2.79×10^{-39} and 2×10^{-15} , respectively (Eqs. 2–7).





It is known that Fe³⁺ and Ni²⁺ begin to precipitate as Fe(OH)₃ and Ni(OH)₂, respectively, at pH = 1.5 and pH = 6.7. At a pH value of 5, Fe(OH)₃ transforms to FeO.OH. Above a pH of 7, the concentration of Ni²⁺ increases and Ni(OH)₂ occurs in the reaction mixture. The Ni(OH)₂ reacts with the FeO.OH to form crystalline NiFe₂O₄ particles.³⁸ The color of the mixture is orange at the beginning but changes to light brown with the increasing pH value. Above a pH of 7, the color transforms to deep brown and precipitation occurs.

Effect of the Mole Ratio of Fe³⁺/Ni²⁺

Several experiments were carried out to examine the effect of mole ratios of Fe³⁺/Ni²⁺ of 1.0, 1.5, 2.0, and 2.5. The pH and ethanolamine volume were kept constant at 8 and 20 mL, respectively. The samples obtained at different mole ratios of Fe³⁺/Ni²⁺ are shown in Fig. 2a–d.

Figure 2a shows the XRD analysis results of the Fe³⁺/Ni²⁺ = 1 sample. This sample consisted of pure Ni_{1.43}Fe_{1.7}O₄ with the ICDD number 800072. It can be expected that NiFe₂O₄ is formed instead of Ni_{1.43}Fe_{1.7}O₄. This can be explained by the mole ratio of Fe³⁺/Ni²⁺ = 1 being inadequate to form NiFe₂O₄ particles.

The XRD results of the sample with a mole ratio of Fe³⁺/Ni²⁺ = 1.5 are given in Fig. 2b. The NiFe₂O₄ compound with the ICDD card number 540964 is seen in Fig. 2b. It was determined by XRD analysis

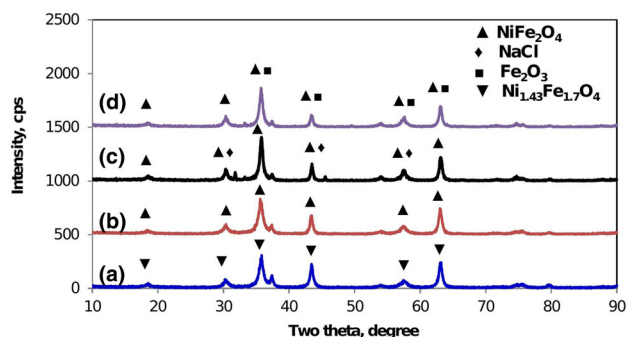


Fig. 2. XRD patterns of the mole ratio of Fe³⁺/Ni²⁺: (a) 1.0, (b) 1.5, (c) 2.0, and (d) 2.5.

that single-phase nickel ferrite was obtained. The average crystallite size (*D*) of the particle of the sample is determined by using the Scherrer formula (Eq. 8).⁴⁰

$$D = \frac{0.9\lambda}{\beta \cos \theta} \quad (8)$$

where *D* is the mean dimension of the crystallite, β is the full width at half-maximum in radians, and λ is the x-ray wavelength, and θ is the Bragg diffraction angle for the actual peak. Utilizing the sharp peak (3 1 1) of NiFe₂O₄ in the form of XRD belonging to the sample with the mole ratio Fe³⁺/Ni²⁺ = 1.5, the mean crystal size was calculated as 108 nm.

Figure 2c shows the XRD peaks of the Fe³⁺/Ni²⁺ = 2 sample. In this graph, NiFe₂O₄ with the ICDD card number 540964 and NaCl compounds with the ICDD number 750306 were observed. NaCl formed as a result of the reaction sample of nickel chloride and iron chloride causing excessive salt formation. NaCl was found as an impurity when it is not washed sufficiently because it is difficult to remove this salt from the precipitate.

The XRD peaks of Fe³⁺/Ni²⁺ = 2.5 sample are given in Fig. 2d. NiFe₂O₄ with the ICDD card number 540964 and Fe₂O₃ compounds with the ICDD card number 330664 were determined. The formation of NiFe₂O₄ and Fe₂O₃ compounds instead of pure NiFe₂O₄ can be attributed to the high Fe³⁺/Ni²⁺ mole ratio. Because of the high mole ratio, the iron also increased.

SEM and EDAX Analysis

Morphology, particle size, and elemental composition of NiFe₂O₄ synthesized via co-precipitation were investigated using SEM. It can be seen from Fig. 3 that plate-shaped NiFe₂O₄ nanoparticles were obtained. In this analysis, the SEM image of

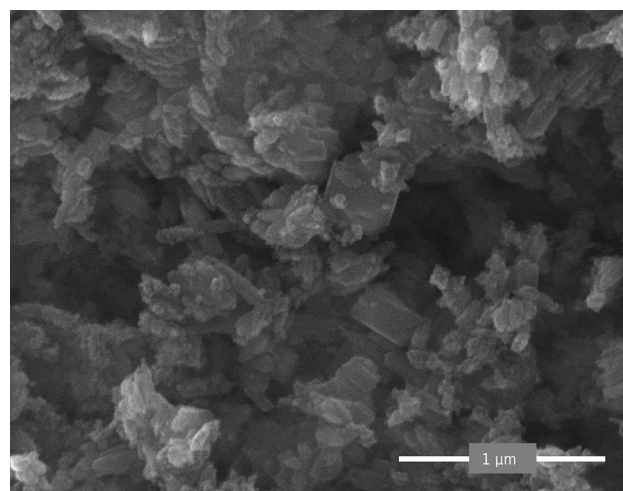


Fig. 3. SEM images of NiFe₂O₄ nanoplate particles calcined at 650°C.

the sample is magnified 100,000 times compared to the original. As a result of the SEM analysis, it was determined that the sample, NiFe_2O_4 was nanometer-sized. This is in good agreement with the results of the XRD analysis. The average particle size of the NiFe_2O_4 nanoparticles was calculated by XRD analysis as 108 nm. The large plate supports the finding that pure NiFe_2O_4 crystals were formed. Iron and nickel chloride salts were successfully converted to nickel ferrite via the calcination process at 650°C . In this SEM analysis, some agglomeration was observed.

Jacob et al.⁴¹ and Li et al.⁴² reported that cluster-like structures are formed due to agglomeration on the surface of plate-shaped crystalline particles. Lattice disorder and strains decrease during the calcination process carried out at high temperature. This results in the coalescence of smaller grains and an increase in the average grain size of the nanoparticles with a wide size distribution. Khan et al.⁴³ stated that one of the factors that gives rise to agglomeration may be electrostatic magnetic attraction.

Solid crystal NiFe_2O_4 formation from solution can be explained by the Ostwald ripening mechanism. Nuclei are formed when the diameter of the particles in the medium is larger than the critical diameter. An embryo is formed when the diameter of the particles in the medium is smaller than the critical diameter. These embryos dissolve again and accumulate on the surface of the nuclei. The surface/volume ratio of the embryos is higher and their surface energy is greater. The surface/volume ratio of the nuclei is small, and therefore their surface energy is lower. Nucleus formation is a reasonable result, since, thermodynamically, systems have a tendency to transform into structures with lower surface energy. In the solution medium, the concentration of large particles at the solution–particle interface is less than the average concentration, and the concentration of small particles at the solution–particle interface is higher than the average concentration. In this case, they diffuse from the dense medium to the less dense environment and collect on the surface, and nucleus growth and subsequent crystal formation takes place. As a result, large-diameter particles use small-diameter particles as “fuel” in crystal formation.^{44,45}

The results of EDAX analysis is shown in Fig. 4. The spectrum of EDAX of the prepared NiFe_2O_4 nanoparticles indicates that the sample only contains oxygen (O), iron (Fe), and nickel (Ni) atoms, and no impurity was observed. The theoretical mole ratio of Ni:Fe:O = 1:2:4 is close to the EDAX mole ratio of Ni:Fe:O = 1.01:2.03:3.84. That is, the molecular formula of the sample derived from co-precipitation is equal to its theoretical value. Table I gives the comparison between the theoretical mole ratio and the mole ratio of the EDAX analysis of NiFe_2O_4 .

Functional Groups Analysis (FTIR)

The FTIR spectrum of the NiFe_2O_4 nanoparticles was taken to determine the chemical structure of the sample. The FTIR spectrum was observed above the frequency range of $4000\text{--}400\text{ cm}^{-1}$, as shown in Fig. 5. In this study, stress vibration frequencies of metal–oxygen bonds formed in tetrahedral and octahedral regions which were found at $K1 = 590\text{ cm}^{-1}$ and $K2 = 408\text{ cm}^{-1}$, respectively. The broad band near 3456 cm^{-1} and the sharp peak near 1638 cm^{-1} correspond to the symmetric stretching and bending vibrations of H–O–H, respectively, due to free or adsorbed water in the form of synthesized NiFe_2O_4 . The peak observed at 802 cm^{-1} is assigned to the deformation vibration of Fe–OH groups. The bands near 1470 , 1034 , and 2333 cm^{-1} are attributed to in-plane and out-plane bending vibrations of O–H bonds, respectively.

The absorption bands below 1000 cm^{-1} belong to the vibration of the metal–oxygen bands.⁴⁶ In reverse spinel nickel ferrites, there are two main regions: the tetrahedral region and the octahedral region.² Fe^{3+} ions occupied both regions, and all the Ni^{2+} ions were located in the B region.⁴⁷ In the tetrahedral region, Fe^{3+} ions are surrounded by four oxygen atoms and form an AO4 structure. In the octahedral region, Ni^{2+} ions are surrounded by six oxygen atoms and the BO6 structure is formed. In the FTIR spectrum of all the spinels, especially nickel ferrites, metal–oxygen bonds are divided into two lower absorption bands.⁴⁸

Vibrating Sample Magnetometer (VSM) Analysis

Hysteresis loops of the synthesized NiFe_2O_4 nanoparticles are shown in Fig. 6. Saturation magnetization (Ms) of the NiFe_2O_4 nanoparticles sample was measured as 14.6 emu/g. Smit and Wijn⁴⁹ reported bulk NiFe_2O_4 saturation magnetization values as 50 emu/g. The saturation magnetization values of NiFe_2O_4 nanoparticles were reported as 18 emu/g,³⁴ 14.22 emu/g,⁴¹ 25 emu/g,⁵⁰ and 23.1 emu/g.²⁴ The Ms value of NiFe_2O_4 nanoparticles is significantly lower than the Ms value of bulk NiFe_2O_4 (55 emu/g). The decrease in saturation magnetization of these samples relative to the bulk material depends on different parameters. In the calcination process, the heating rate of the furnace is one of the most important parameters that can increase or decrease the saturation magnetization. It is a high heating rate when the heating rate of calcination is $10^\circ\text{C}/\text{min}$. It is possible to obtain higher crystallization by calcination at a slow heating rate. The lower Ms value of the synthesized samples compared to the Ms value of the bulk sample was attributed to the larger fraction of the surface turns in these nanoparticles.⁴³

Remanent magnetization of the sample was measured to be 2.3 emu/g. In the literature, remanent

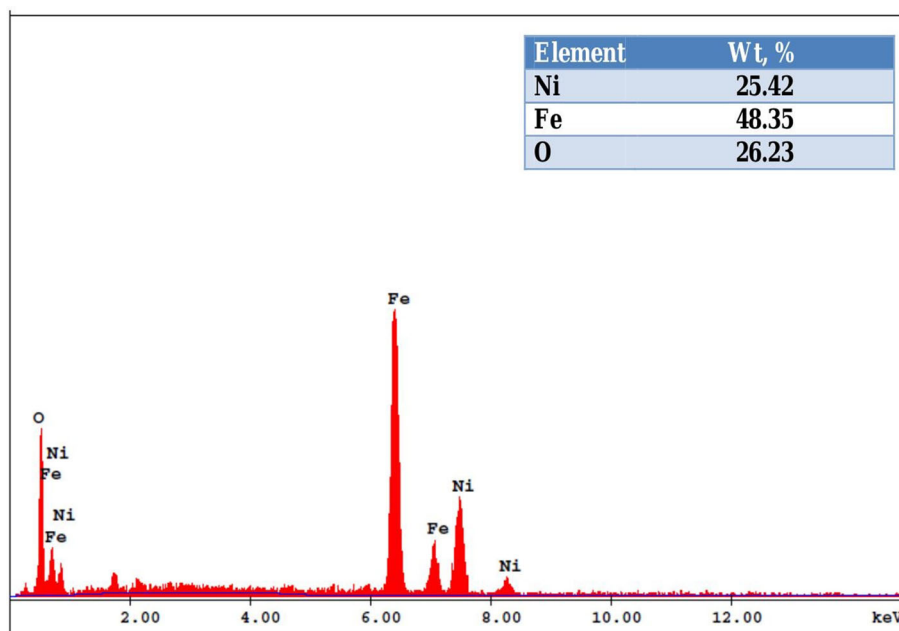


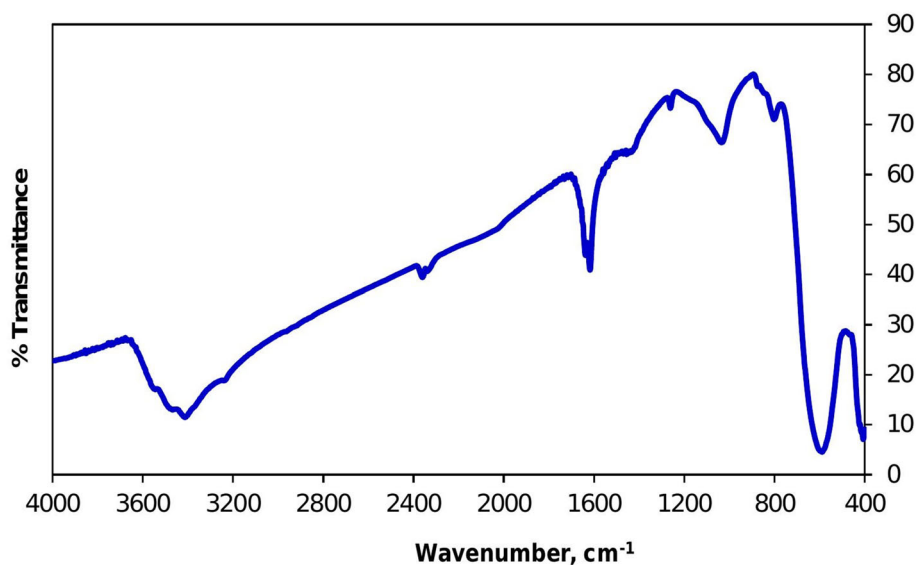
Fig. 4. EDAX analysis of nickel ferrite nanoparticles.

Table I. Theoretical mole ratio of NiFe₂O₄ and mole ratio of EDAX analysis of the sample

| Element | Theoretical mole ratio | EDAX mole ratio |
|---------|------------------------|-----------------|
| Ni | 1 | 1.0152 |
| Fe | 2 | 2.0292 |
| O | 4 | 3.8424 |

magnetization values of NiFe₂O₄ nanoparticles have been reported as 2.45 emu/g⁷ and 3.88 emu/g.⁴¹

In this study, the coercivity of NiFe₂O₄ plate nanoparticles was measured as 288 Oe. NiFe₂O₄ plate nanoparticles showed ferrimagnetic behavior at room temperature. Many soft magnetic materials are relatively easy to demagnetize, beginning to demagnetize when the applied magnetic field is

Fig. 5. FTIR spectra of NiFe₂O₄ nanoparticles.

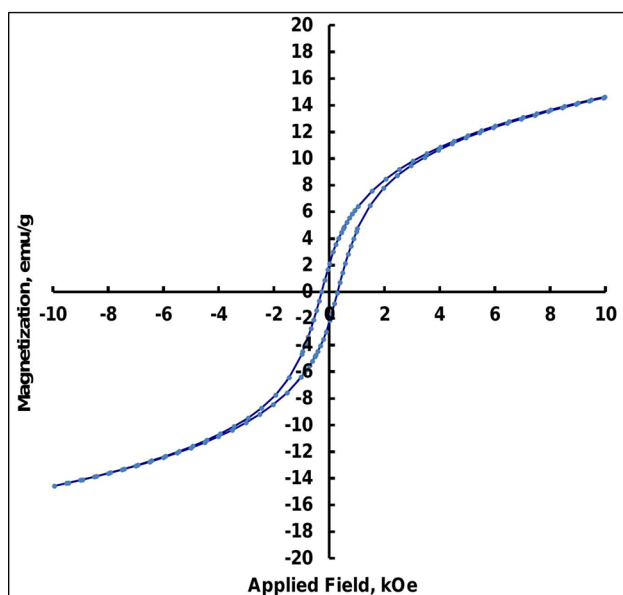


Fig. 6. Hysteresis loops of synthesized NiFe_2O_4 nanoparticles.

removed. Therefore, soft magnetic materials are easily magnetized and demagnetized. Laokul et al.⁵⁰ reported the coercivity value of 26-nm particle size NiFe_2O_4 nanoparticles synthesized by the sol-gel method as 289 Oe. The coercivity of the NiFe_2O_4 nanoparticles was determined as 245.5 Oe,²⁴ 205 Oe,¹ and 675 Oe.⁵¹

CONCLUSION

The synthesis and characterization of nickel ferrite (NiFe_2O_4) plate nanoparticles by co-precipitation have been investigated. NiFe_2O_4 plate nanoparticles with 108-nm particle size were successfully synthesized using the $\text{Fe}^{3+}/\text{Ni}^{2+} = 2$ mole ratio. The resulting sample was confirmed to be pure crystalline NiFe_2O_4 by EDAX and XRD analyses. In the synthesis process with $\text{Fe}^{3+}/\text{Ni}^{2+} = 1$ mole ratio, a $\text{Ni}_{1.43}\text{Fe}_{1.7}\text{O}_4$ compound was formed where NiFe_2O_4 was expected to form. In the synthesis process at pH = 7 and pH = 10, NiFe_2O_4 and Fe_2O_3 compounds were also formed. However, at pH = 8 and pH = 9, only the NiFe_2O_4 phase was formed and no impurity was observed. SEM, XRD, and EDAX analyses showed that samples calcined at 650°C were well-crystallized pure NiFe_2O_4 plate nanoparticles. Magnetic analysis showed that the synthesized NiFe_2O_4 nanoplate particles had a saturation magnetization value of 14.6 emu/g and a coercivity of 288 Oe. Accordingly, synthesized NiFe_2O_4 plate nanoparticles have ferrimagnetic properties, and NiFe_2O_4 plate nanoparticles showed soft magnetic behavior.

CONFLICT OF INTEREST

The authors declare that they have no conflict of interest. There has been no financial support for this study that could have influenced its outcome.

REFERENCES

- P. Sivakumar, R. Ramesh, A. Ramanand, S. Ponnusamy and C. Muthamizhchelvan, *Mater. Lett.* 65, 483. (2011).
- K.S.A. Kumar and R.N. Bhowmik, *Mater. Chem. Phys.* 146, 159. (2014).
- C.N. Chinnasamy, A. Narayanasamy, N. Ponpandian, K. Chattopadhyay, K. Shinoda, B. Jeyadevan, K. Tohji, K. Nakatsuka, T. Furubayashi and I. Nakatani, *Phys. Rev. B* 63, 184108. (2001).
- M. McHenry and D. Laughlin, *Acta Mater.* 48, 223. (2000).
- S. Roy, I. Dubenko, D.D. Ederh and N. Ali, *J. Appl. Phys.* 96, 1202. (2004).
- J. Jacob and M.A. Khadar, *J. Appl. Phys.* 107, 114310. (2010).
- S. Joshi, M. Kumar, S. Chhoker, G. Srivastava, M. Jewariya and V.N. Singh, *J. Mol. Struct.* 1076, 55. (2014).
- M. Rashad and O. Fouad, *Mater. Chem. Phys.* 94, 365. (2005).
- J.A.C. Arango, A.A. Cristobal, C.P. Ramos, P.G. Bercoff and P.M. Botta, *J. Alloys Compd.* 811, 152044. (2019).
- M. Younas, M. Nadeem, M. Atif and R. Grossinger, *J. Appl. Phys.* 109, 093704. (2011).
- S. Thakur, R. Rai and S. Sharma, *Mater. Lett.* 139, 368. (2015).
- A. Ceylan, S. Ozcan, C. Ni and S.I. Shah, *J. Magn. Magn. Mater.* 320, 857. (2008).
- M. Khairy and M.E. Gouda, *J. Adv. Res.* 6, 555. (2015).
- D. Lin, A.C. Nunes, C.F. Majkrzak and A.E. Berkowitz, *J. Magn. Magn. Mater.* 145, 343. (1995).
- S.A. Oliver, V.G. Harris, H.H. Hamdeh and J.C. Ho, *Appl. Phys. Lett.* 76, 2761. (2000).
- Y. Shi and J. Ding, *J. Appl. Phys.* 90, 4078. (2001).
- C.N. Chinnasamy, A. Narayanasamy, N. Ponpandian, R. Justin Joseyphus, B. Jayadevan, K. Tohji and K. Chattopadhyay, *J. Magn. Magn. Mater.* 238: 281 (2002).
- T. Abraham, *Am. Ceram. Soc. Bull.* 73, 62. (1994).
- R. Dehghan, S. Seyyed Ebrahimi, A. Badiei and J. Non-Cryst, *Solids* 354, 5186. (2008).
- T. Shanmugavel, S.G. Raj, G.R. Kumar, G. Rajarajan and D. Saravanan, *J. King Saud Univ. Sci.* 27, 176. (2015).
- P. Deb, A. Basumallick and S. Das, *Solid State Commun.* 142, 702. (2007).
- J. Wang, F. Ren, R. Yi, A. Yan, G. Qiu and X. Liu, *J. Alloys Compd.* 479, 791. (2009).
- K. Maaz, S. Karim, A. Mumtaz, S.K. Hasanain, J. Liu and J.L. Duan, *J. Magn. Magn. Mater.* 321, 1838. (2009).
- M. Salavati-Nasari, F. Davar and T. Mahmoudi, *Polyhedron* 28, 1455. (2009).
- B. Baruwati, R.K. Rana and S.V. Manorama, *J. Appl. Phys.* 101, 14302. (2007).
- P. Chand, S. Vaish and P. Kumar, *Phys. B* 524, 53. (2017).
- A.M. Dumitrescu, A.I. Borhan, A.R. Iordan, I. Dumitru and M.N. Palamaru, *Powder Technol.* 268, 95. (2014).
- A. Sutka, R. Parna, T. Kaambre and V. Kisand, *Phys. B* 456, 232. (2015).
- A. Azizi and S.K. Sadrnezhaad, *Ceram. Int.* 36, 2241. (2010).
- J. Fang, N. Shama, L.D. Tung, E.Y. Shin, C.J. Oconnor, K.L. Stokes, G. Caruntu, J.B. Wiley, L. Spinu and J. Tang, *J. Appl. Phys.* 93, 7483. (2003).
- S. Balaji, R.K. Selvan, L.J. Berchmans, S. Angappan, K. Subramanian and C.O. Augustin, *Mater. Sci. Eng. B* 119, 119. (2005).
- M.A.S. Amulya, H.P. Nagaswarupa, M.R.A. Kumar, C.R. Ravikumar, S.C. Prashantha and K.B. Kusuma, *Appl. Surf. Sci. Adv.* 1, 100023. (2020).
- A.Y. Baranchikov, V.K. Ivanov and Y.D. Tretyakov, *Ultrason. Sonochem.* 14, 131. (2007).
- U. Kurtan, H. Gungunes, H. Sozeri and A. Baykal, *Ceram. Int.* 42, 7987. (2016).
- S.K. Pradhan, S. Bid, M. Gateshki and V. Petkov, *Mater. Chem. Phys.* 93, 224. (2005).
- N. Gupta, P. Jain, R. Ran and S. Shrivastava, *Mater. Today Proc.* 4, 342. (2017).

37. Z. Zhu, X. Li, Q. Zhao, H. Li, Y. Shen and G. Chen, *Chem. Eng. J.* 165, 64. (2010).
38. A. Shan, X. Wu, J. Lu, C. Chen and R. Wang, *CrytEngComm* 17, 1603. (2015).
39. S.H. Lafta, *Open Chem.* 15, 53. (2017).
40. P. Scherrer, *Abh. Ges. Wiss. Goettingen Math. Phys.* 2, 98. (1918).
41. B.P. Jacob, A. Kumar, R.P. Pant, S. Singh and E.M. Mohammed, *Bull. Mater. Sci.* 34, 1345. (2011).
42. J. Li, Y. Lin, X. Liu, Q. Zhang, H. Miao, T. Zhang and B. Wen, *Phase Trans.* 84, 49. (2011).
43. A.A. Khan, M. Javed, A.R. Khan, Y. Iqbal, A. Majeed, S.Z. Hussain and S.K. Durrani, *Mater. Sci. Pol.* 35, 58. (2017).
44. P.W. Voorhees, *J. Stat. Phys.* 38, 231. (1985).
45. J.A. De Chalendar, C. Garing and S.M. Benson, *J. Fluid Mech.* 835, 363. (2018).
46. K. Kombaiah, J.J. Vijaya, L.J. Kennedy and K. Kaviyarasu, *Mater. Chem. Phys.* 221, 11. (2019).
47. F.L. Zabotto, A.J. Gualdi, J.A. Eiras, A.J.A. de Oliveira and D. Garcia, *Mater. Res.* 15, 428. (2012).
48. R. Kesavamoorthi, A.N. Vigneshwaran, V. Sanyal and C.R. Raja, *J. Chem. Pharm. Sci.* 9, 160. (2016).
49. J. Smit and H.P.J. Wijn, *Ferrites* (Cleaver-Hume, London, 1959).
50. P. Laokul, V. Amornkitbamrung, S. Seraphin and S. Maensiri, *Curr. Appl. Phys.* 11, 101. (2011).
51. L. Chen, H. Dai, Y. Shen and J. Bai, *J. Alloys Compd.* 491, L33. (2010).

Publisher's Note Springer Nature remains neutral with regard to jurisdictional claims in published maps and institutional affiliations.